Electronic Supplementary Material (ESI) for Environmental Science: Advances.

Linear perfluoroalkyl carboxylate reduction dynamics with solvated electrons from ferrocyanide and sulfite.

William A. Maza*, James A. Ridenour, Brian L. Chaloux, Jeffrey C. Owrutsky, and Albert Epshteyn

Chemistry Division, US Naval Research Laboratory, Washington, D.C. 20375
National Research Council, Chemistry Division, US Naval Research Laboratory, Washington, D.C. 20375

Contents:

Single Crystal Analysis

X-ray diffraction quality crystals of NaPF8A were obtained by layering a 80mM aqueous solution of NaPF8A onto 1M NaCl in water and were used for the structural analysis. A colorless rod-shaped crystal was mounted on a MiTeGen micromount. Reflection data were collected at 100(2) K with 0.5 °ω scans on a Bruker D8 Quest diffractometer equipped with a Photon II detector using Mo Kα (λ = 0.71073) radiation. The data were integrated using the SAINT program within the APEX III software suite and an absorption correction was applied using SADABS.[1] The crystal structure of NaPF8A was solved *via* intrinsic phasing using ShelXT[2] and refined using ShelX-2018/3[3] within the APEX III suite. All atoms were located in the difference Fourier map and refined anisotropically. The hydrogen atoms on the ten interstitial water molecules were not found in the Fourier map, and efforts to place them at idealized positions were unsuccessful. Positional disorder in several of the PF8A chains were modeled in two parts using PART, SIMU, and RIGU commands. The structure was checked for additional symmetry using PLATON.[4] The NaPF8A structure was visualized with Mercury and figures were prepared with CrystalMaker. A thermal ellipsoid figure, generated using the ORTEP software,[5] is available in Figures S7. Tables of bond distances are also available in Table S3.

^{19}F Diffusion-Ordered NMR Spectroscopy (^{19}F-DOSY). NMR experiments were performed on a Bruker AVANCE NEO 400 MHz (9.4 T) spectrometer equipped with a broadband probe operating at 376.498 MHz for ^{19}F. Solutions of sodium perfluorooctanoate ($NaOOC_8F_{15}$, PFOA) were prepared at 100 μM and 4 mM concentration in 4:1 H_2O:D_2O mixture. Experiments were performed in 5 mm borosilicate glass NMR tubes without sample spinning while holding sample temperature at 298 ± 1 K. The ^{19}F 90° pulse angle for PFOA was measured to be 17.5 μs for both samples. Data were processed using a combination of Bruker TopSpin 4.0.9 (Figure S3) and OriginPro 2020 (Figure S2).

A Oneshot45 pulse sequence utilizing unbalanced bipolar pairs of smoothed square gradient pulses (unbalancing factor $\alpha = 0.2$) and a terminal 45° purge pulse was used to collect series of 16 spectra from -75 to -135 ppm (vs. $CFCl_3$) at different applied z-axis gradient strengths (2.4–38.5 G cm^{-1}). To achieve sufficient signal-to-noise, 720 scans (+ 4 dummy scans) were collected per spectrum using a 1 s acquisition time (aq) and 2 s relaxation delay (d1). A 0.2 ms gradient recovery delay (d16) was applied between gradients. 25 Hz of line broadening were applied when processing spectra to further improve signal-to-noise. For the 100 μM PFOA solution, a gradient pulse pair length (δ = 2×p30) of 1 ms and evolution time (Δ = d20) of 0.1 s were used; for the 4 mM sample, gradient length (δ) was set to 2 ms and evolution time (Δ) to 0.5 s, resulting in more complete attenuation at high gradient strength.

The DOSY AU program included in TopSpin was utilized to prepare Figure S3 from the series of spectra as a function of applied z-gradient strength. To more accurately calculate diffusion coefficients using external software (OriginPro), the series of spectra were processed using the T1T2 routine in TopSpin, integrating the 7 ^{19}F peaks originating from distinct CF_2 and CF_3 species. Peak integrations were exported to text files, imported into Origin, and fit to the Stejskal-Tanner equation:

$$I = I_0 e^{-DG^2(2\pi\gamma)^2\delta^2\Delta}$$

5

where I_0 is the integrated intensity in the absence of an applied gradient, D is the diffusion coefficient, G is the gradient strength, γ is the gyromagnetic ratio of the nucleus being probed (^{19}F = 4007.8 Hz/G), and δ and Δ are pulse program parameters as defined above. The results of these analyses are presented in Figure S2.

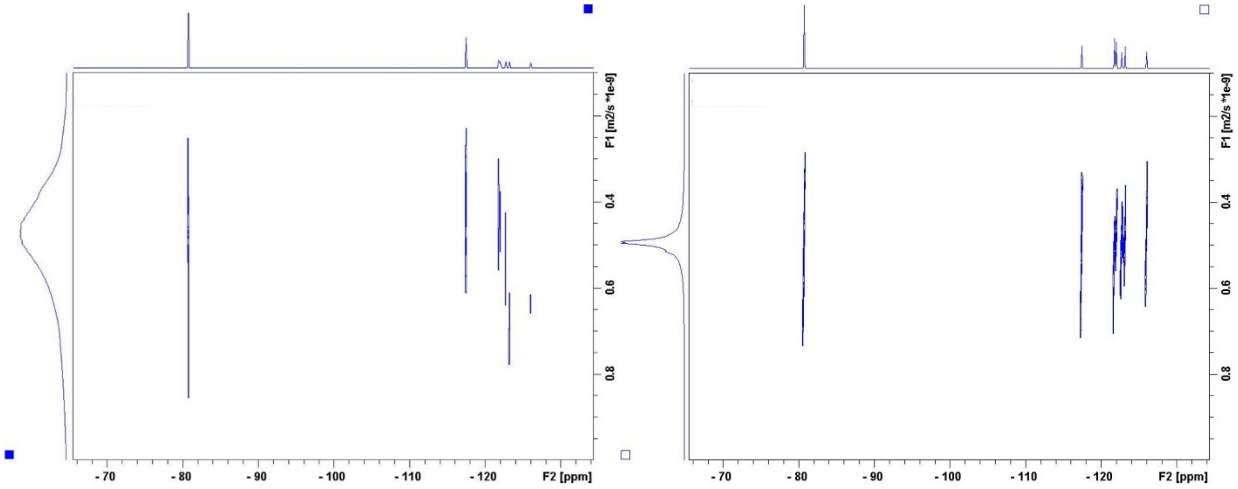

Figure S1. Processed ^{19}F DOSY NMR spectra of PFOA in D_2O at pH 10 at two different concentrations (left panel = 100 μM PFOA, right panel = 4 mM PFOA). Relative errors in calculated diffusion coefficients are represented by the 'width' of the peaks in the diffusion (y-) axis. Projections of the integrated diffusion coefficients (left) and integrated peak intensities (top) are shown beside each spectrum; due to improved signal-to-noise, error bars are smaller in the 4 mM spectrum than the 100 μM spectrum.

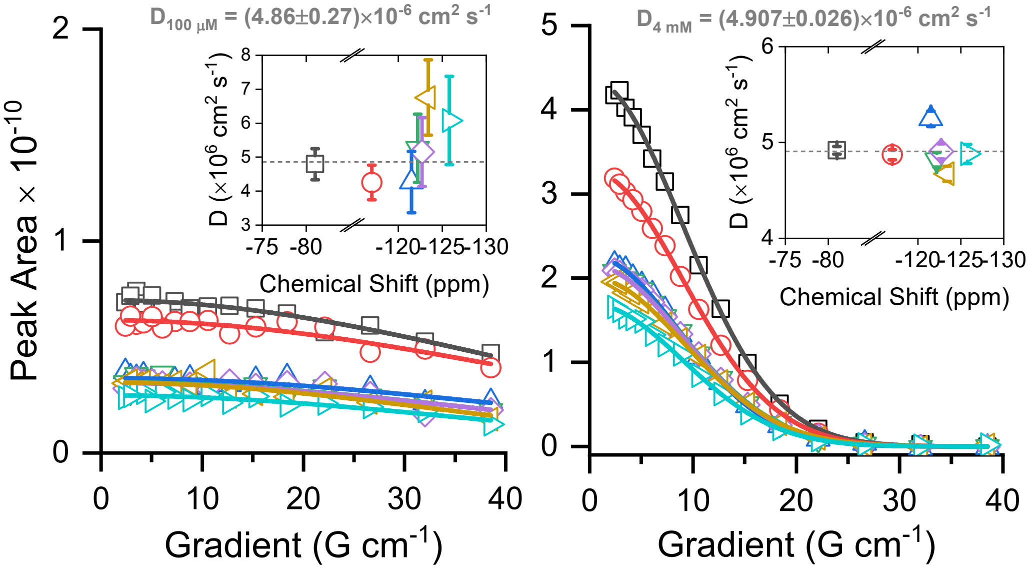

Figure S2. Plots of integrated peak intensity for each of the ^{19}F peaks in the spectra presented in Figure S3 (left panel = 100 μM PFOA, right panel = 4 mM PFOA) versus applied gradient strength. Data are fit (solid lines) to a Stejskal-Tanner model to extract diffusion coefficients, which are plotted in the inset figures vs. the ^{19}F chemical shift of the peaks in question. Average diffusion coefficients (grey text) are calculated from global fits to each set of ^{19}F peaks where D is shared between peaks and plotted (dashed grey horizontal line) in the inset figures for reference. Most diffusion coefficients calculated from individual peaks are within error of the average diffusion coefficient calculated from all peaks. Fitting a single diffusion coefficient to all 7 peaks in aggregate yields $D_{100\ \mu M} = (4.86\pm0.27)\times10^{-6}$ cm^2 s^{-1} and $D_{4\ mM} = (4.91\pm0.03)\times10^{-6}$ cm^2 s^{-1}. Within error, there is thus no change in the average diffusivity of PFOA across the concentration ranges explored in this manuscript. Fits of individual peaks yield diffusion coefficients that are within error of the global fits.

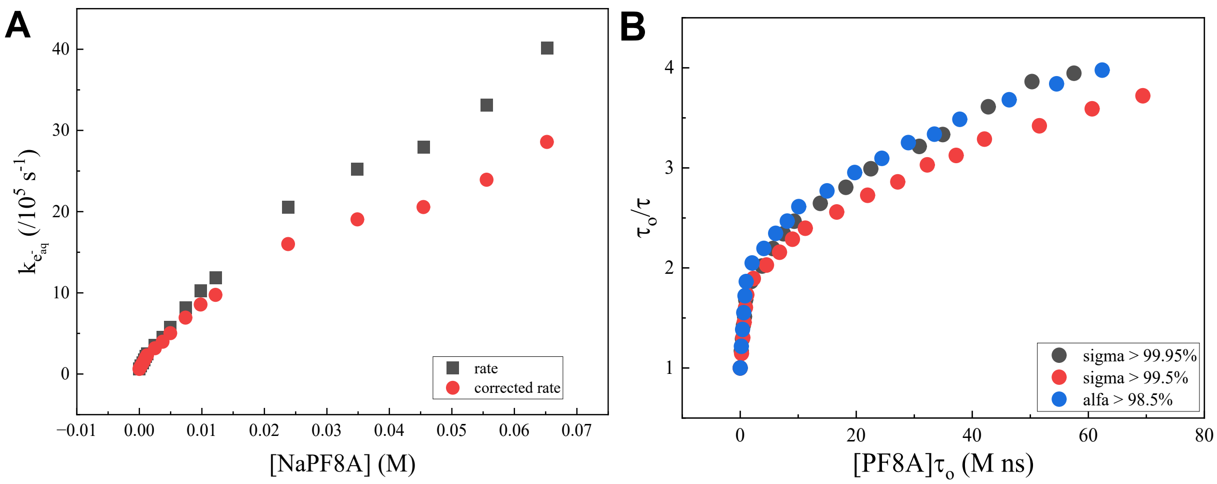

Figure S3. (A) Hydrated electron decay rate as a function of [NaPF8A] in a 40 mM borate buffer solution containing 40 μM $K_4Fe(CN)_6$ before (black squares) and after (red circles) correcting for the change in ionic strength. (B) Modified Stern-Volmer plot of the dependence of the e_{aq}^- decay rate on the [NaPF8A] in aqueous solutions of $Fe(CN)_6^{4-}$ (in the absence of borate buffer) prepared from two different manufacturers and three different levels of purity.

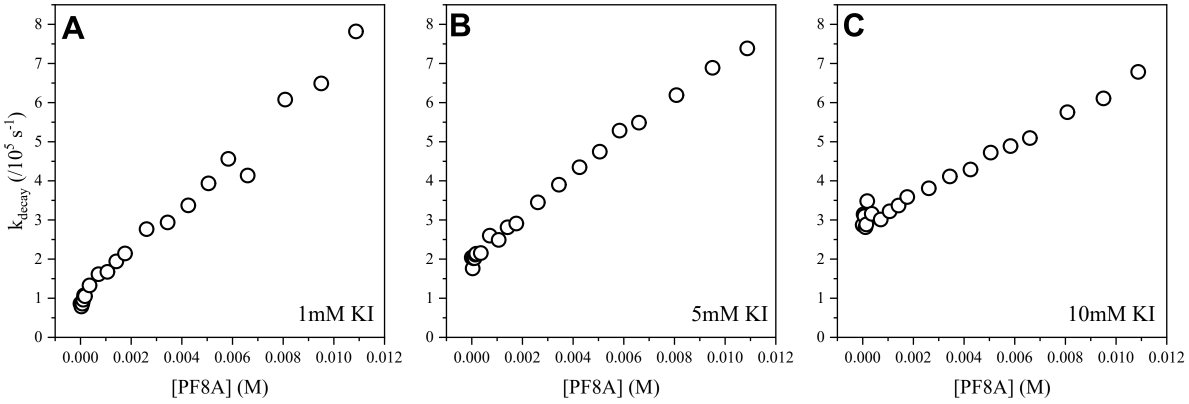

Figure S4. Modified Stern-Volmer plots of the dependence of the e_{aq}^- decay rate on the [NaPF8A] in aqueous solutions of (A) 1 mM KI, (B) 5 mM KI, and (C) 10 mM KI.

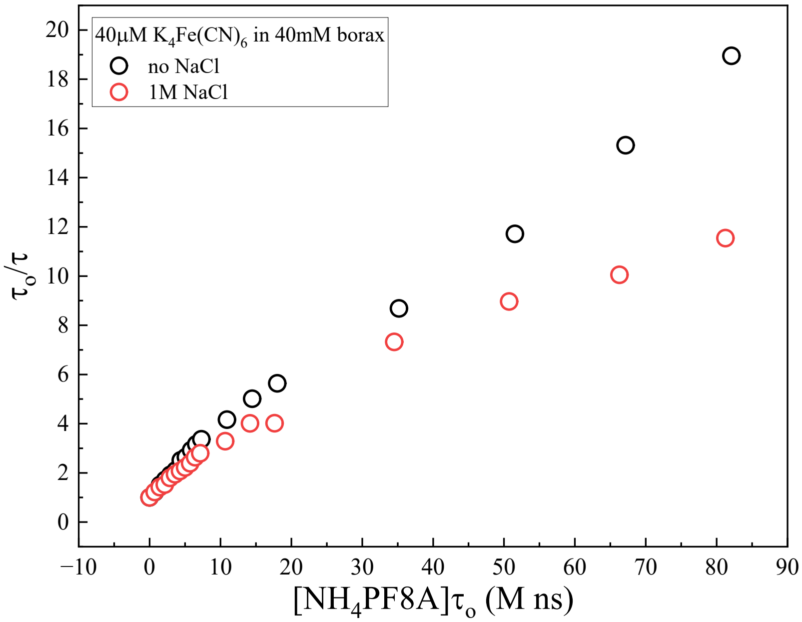

Figure S5. Modified Stern-Volmer plot of the e_{aq}^- decay rate dependence on the [NH$_4$PF8A] in the absence (black) and presence (red) of 1 M NaCl.

Derivation of Dimerization UV-visible Absorbance Model

Assuming the following equilibrium

$$2PFOA \overset{K_a}{\leftrightarrow} PFOA_2 \qquad \text{S1}$$

having an expression for the equilibrium constant of dimerization, K$_a$,

$$K_a = \frac{[PFOA_2]_{eq}}{[PFOA]_{eq}^2} = \frac{c_d}{c_m^2} \qquad \text{S2}$$

where [PFOA$_2$]$_{eq}$ and c_d are the equilibrium concentration of PFOA dimer, [PFOA]$_{eq}$ and c_m are the equilibrium concentration of PFOA monomers. The total concentration of PFOA, c_o, is

$$c_o = c_m + 2c_d \qquad \text{S3}$$

Equation S2 can be rearranged to solve for both c_m and c_d in terms of c_o and K$_a$

$$c_m = \frac{\sqrt{1 + 8K_a c_o} - 1}{4K_a} \qquad \text{S4}$$

$$c_d = \frac{2 - 2\sqrt{1 + 8K_a c_o} + 8K_a c_o}{16K_a} \qquad \text{S5}$$

In the Beers-Lambert regime at any given wavelength the total absorbance, A_{tot}, is less than 1, the A_{tot} can be approximated as the sum of the contributions from the absorbance of PFOA monomer species, A_m, and dimer, A_d.

$$A_{tot,\lambda} = A_m + A_d \qquad \text{S6}$$

$$A_{tot,\lambda} = \varepsilon_\lambda c_o = \varepsilon_m c_m + \varepsilon_d c_d \qquad \text{S7}$$

In S7 ε_i is the molar extinction coefficient of the respective monomer or dimer. For simplicity, both S6 and S7 assume that all the various dimer configurations have similar values of ε_d which we believe is reasonable. Substituting S3 and S4 into S7, then rearranging and simplifying we arrive at an expression for the total absorbance in terms of c_o and K_a

$$A_{tot,\lambda} = \frac{\varepsilon_d c_o}{2} + \left(\varepsilon_m - \frac{\varepsilon_d}{2}\right)\left\{\frac{\sqrt{1+8K_a c_o} - 1}{4K_a}\right\} \qquad \text{S8}$$

To facilitate data analysis, ε_m can be estimated by a Beers-Lambert analysis of the absorbance of PFOA as sufficiently small concentrations.

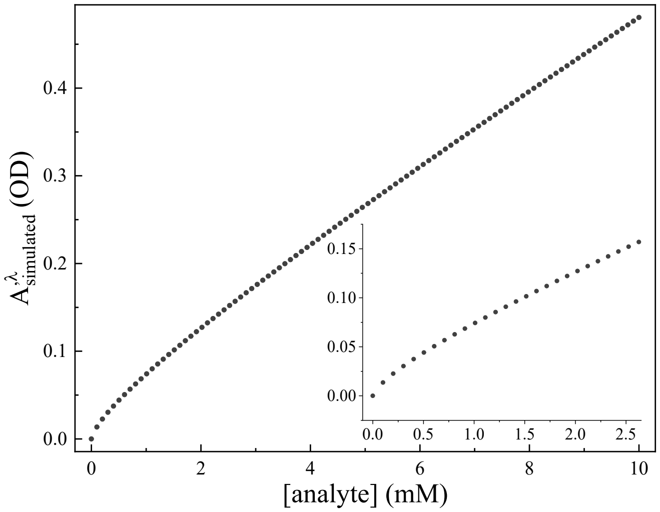

Figure S6. Simulated absorbance for the simple aggregation of an analyte according to equation S8 demonstrating the nonlinear dependence of the absorbance on the analyte concentration, where the molar extinction coefficients of the monomer and dimer at a given wavelength are 260 M^{-1} cm^{-1} and 70 M^{-1} cm^{-1}, respectively with equilibrium constant of dimerization K_a of 14000 M^{-1}. The inset shows the same simulated data zoomed in to the lower concentration range where the data deviates from Beer's-Lambert behavior. The value of ε_m used in the simulation was estimated from the experimental absorbance of NaPF8A at 40 µM whereas the value of K_a used in the simulation was based on the previously reported value.[6]

Rate Constants for Different Quenchers

Table S1. Summary of the apparent rate constants k_{NaPFxA} obtained in aqueous solutions of $Fe(CN)_6^{4-}$, SO_3^2, and indole.

	k_{NaPFxA} (1mM < [NaPFxA] < 10mM, M^{-1} s^{-1})			
	40 µM $Fe(CN)_6^{4-}$	10 mM SO_3^{2-}	80 µM Indole	10 mM KI
NaPF8A	$(6.6\pm0.9)\times10^7$	$(5.6\pm0.2)\times10^7$	$(1.0\pm0.1)\times10^8$	$(3.5\pm0.5)\times10^7$
NaPF7A	$(1.9\pm0.1)\times10^7$	$(2.0\pm0.1)\times10^7$	$(3.1\pm0.1)\times10^7$	

NaPF6A	$(3.4\pm0.1)x10^{7}$	$(2.9\pm0.2)x10^{7}$	$(3.7\pm0.6)x10^{7}$	
NaPF5A	$(1.8\pm0.1)x10^{7}$	$(1.0\pm0.1)x10^{7}$	$(1.9\pm0.4)x10^{7}$	
NaPF4A	$(3.7\pm0.2)x10^{7}$	$(2.0\pm0.2)x10^{7}$	$(5.0\pm0.1)x10^{7}$	

Crystal Structure Determined for NaPF8A

We also used other approaches to assess counterion effects in PF8A that can influence both ion pairing and aggregation, which can in turn impact the measured rate constants. We attempted to grow crystals and perform crystallography on NH_4PF8A and NaPF8A. Layering an aqueous solution of NaPF8A over 1M NaCl in water produced crystallites of sufficient quality for crystallographic analysis. It was found that the aggregation of PF8A into crystallites is mediated by Na^+ such that the carboxylates of neighboring PF8A are bridged by Na^+ (Figure S7). Similar attempts to produce NH_4PF8A crystals of crystallographic quality did not produce crystals, which may further suggests an inherent difference in the strength of interaction between the Na^+ and PF8A compared to NH_4^+. This, in turn, may explain a significant difference in the extent of aggregation of the Na^+ and NH_4^+ salts.

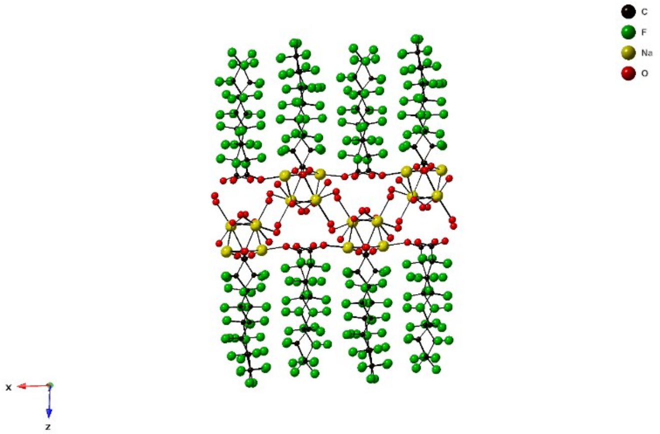

Figure S7. Crystallographic structure of NaPF8A.

Table S2. Table of crystallographic data for NaPF8A.

	1
Formula	$Na_4[C_8F_{15}O_2]_4 \bullet 10H_2O$
Formula Weight	1924.33
Crystal System	Triclinic
Space Group	$P\bar{1}$
a (Å)	9.9748(10)
b (Å)	11.5641(11)
c (Å)	28.506(3)
α (°)	81.274(4)
β (°)	85.618(4)
γ (°)	89.756(4)
Vol (Å^3)	3240.5(6)
Z	2
ρ (g cm^{-3})	1.961
μ (mm^{-1})	0.279
R_{int}	0.0294
R_1	0.1258
wR_2	0.3334

Table 3. Table of carbon-fluorine bond distances. "B" refer to the second 'part' of the position disorder of the PF8A chains. All values are in angstroms (Å).

C2	F1	1.36(3)	C12	F21	1.34(2)	C22B	F40B	1.35(3)
C2B	F1B	1.36(5)	C12B	F21B	1.35(3)	C23	F41	1.32(3)
C2	F2	1.39(2)	C13	F22	1.34(3)	C23B	F41B	1.31(3)
C2B	F2B	1.39(4)	C13B	F22B	1.33(3)	C23	F42	1.33(3)
C3	F3	1.336(19)	C13	F23	1.35(2)	C23B	F42B	1.36(3)
C3B	F3B	1.33(3)	C13B	F23B	1.36(3)	C24	F43	1.36(4)
C3	F4	1.34(2)	C14	F24	1.36(3)	C24B	F43B	1.36(4)
C3B	F4B	1.34(3)	C14B	F24B	1.36(3)	C24	F44	1.30(4)
C4	F5	1.348(19)	C14	F25	1.33(3)	C24B	F44B	1.30(3)
C4B	F5B	1.35(3)	C14B	F25B	1.33(3)	C24	F45	1.33(3)
C4	F6	1.344(19)	C15	F26	1.30(3)	C24B	F45B	1.33(4)
C4B	F6B	1.34(3)	C15B	F26B	1.31(3)	C26	F46	1.37(4)
C5	F7	1.349(19)	C15	F27	1.33(3)	C26B	F46B	1.38(3)
C5B	F7B	1.34(3)	C15B	F27B	1.34(4)	C26	F47	1.36(4)
C5	F8	1.32(2)	C16	F28	1.37(4)	C26B	F47B	1.36(3)
C5B	F8B	1.34(3)	C16B	F28B	1.36(4)	C27	F48	1.35(3)
C6	F9	1.32(2)	C16	F29	1.29(4)	C27B	F48B	1.34(2)
C6B	F9B	1.31(3)	C16B	F29B	1.29(4)	C27	F49	1.35(3)
C6	F10	1.35(2)	C16	F30	1.32(3)	C27B	F49B	1.35(2)
C6B	F10B	1.34(3)	C16B	F30B	1.32(3)	C28	F50	1.35(3)
C7	F11	1.35(3)	C18	F31	1.34(4)	C28B	F50B	1.35(2)
C7B	F11B	1.36(4)	C18B	F31B	1.34(3)	C28	F51	1.34(3)
C7	F12	1.34(3)	C18	F32	1.36(4)	C28B	F51B	1.33(2)
C7B	F12B	1.34(4)	C18B	F32B	1.36(3)	C29	F52	1.35(3)
C8	F13	1.40(3)	C19	F33	1.35(3)	C29B	F52B	1.36(2)
C8B	F13B	1.41(5)	C19B	F33B	1.35(3)	C29	F53	1.35(3)

C8	F14	1.23(4)	C19	F34	1.34(3)	C29B	F53B	1.34(2)
C8B	F14B	1.22(4)	C19B	F34B	1.33(3)	C30	F54	1.31(3)
C8	F15	1.36(3)	C20	F35	1.35(3)	C30B	F54B	1.32(2)
C8B	F15B	1.36(4)	C20B	F35B	1.35(3)	C30	F55	1.34(4)
C10	F16	1.36(3)	C20	F36	1.33(3)	C30B	F55B	1.32(2)
C10B	F16B	1.36(3)	C20B	F36B	1.34(2)	C31	F56	1.36(4)
C10	F17	1.36(3)	C21	F37	1.34(3)	C31	F57	1.25(3)
C10B	F17B	1.37(3)	C21B	F37B	1.33(3)	C31B	F56B	1.36(3)
C11	F18	1.35(2)	C21	F38	1.33(3)	C31B	F57B	1.35(3)
C11B	F18B	1.36(3)	C21B	F38B	1.34(3)	C32	F58	1.35(4)
C11	F19	1.35(2)	C22	F39	1.32(3)	C32	F59	1.30(4)
C11B	F19B	1.36(3)	C22B	F39B	1.34(3)	C32	F60	1.36(4)
C12	F20	1.36(2)	C22	F40	1.37(3)	C32B	F58B	1.33(4)
C12B	F20B	1.36(3)	C22B	F40B	1.35(3)	C32B	F59B	1.31(3)

Table S3. Table of carbon-carbon bond distances. “B” refer to the second ‘part’ of the position disorder of the PF8A chains. All values are in angstroms (Å).

C1	C2	1.533(19)	C11B	C12B	1.55(2)	C21B	C22B	1.55(2)
C1	C2B	1.54(3)	C12	C13	1.56(2)	C22	C23	1.54(3)
C2	C3	1.55(2)	C12B	C13B	1.55(2)	C22B	C23B	1.56(3)
C2B	C3B	1.55(4)	C13	C14	1.55(2)	C23	C24	1.55(3)
C3	C4	1.56(2)	C13B	C14B	1.55(3)	C23B	C24B	1.54(3)
C3B	C4B	1.56(3)	C14	C15	1.56(3)	C25	C26B	1.550(19)
C4	C5	1.55(2)	C14B	C15B	1.55(3)	C25	C26	1.55(3)
C4B	C5B	1.54(3)	C15	C16	1.56(3)	C26	C27	1.52(3)
C5	C6	1.55(2)	C15B	C16B	1.56(3)	C26B	C27B	1.52(2)
C5B	C6B	1.54(3)	C17	C18B	1.57(2)	C27	C28	1.54(3)
C6	C7	1.57(2)	C17	C18	1.57(2)	C27B	C28B	1.55(2)
C6B	C7B	1.56(3)	C18	C19	1.55(3)	C28	C29	1.57(3)
C7	C8	1.55(3)	C18B	C19B	1.56(3)	C28B	C29B	1.56(2)
C7B	C8B	1.54(3)	C19	C20	1.56(3)	C29	C30	1.55(3)
C9	C10	1.56(2)	C19B	C20B	1.56(2)	C29B	C30B	1.55(2)
C9	C10B	1.56(2)	C20	C21	1.55(3)	C30	C31	1.53(3)
C10	C11	1.54(3)	C20B	C21B	1.55(2)	C30B	C31B	1.53(2)
C10B	C11B	1.53(3)	C20B	C21B	1.55(2)	C31B	C32B	1.54(3)
C11	C12	1.55(2)	C21	C22	1.55(3)			

Table S4. Table of carbon-oxygen bond distances. All values are in angstroms (Å).

O1	C1	1.258(10)	O4	C9	1.227(10)	O7	C25	1.245(10)
O2	C1	1.234(10)	O5	C17	1.232(10)	O8	C25	1.230(10)
O3	C9	1.248(10)	O6	C17	1.238(10)			

Table S5. Table of sodium-oxygen, sodium-sodium, or sodium-fluorine distances. “B” refer to the second ‘part’ of the position disorder of the PF8A chains. All values are in angstroms (Å).

Na1	O3	2.187(7)	Na2	O4	2.381(6)	Na4	OW8	2.492(7)
Na1	O2	2.235(7)	Na2	OW5	2.417(7)	Na4	Na1	3.423(4)
Na1	O8	2.241(7)	Na2	OW4	2.418(7)	Na3	O7	2.193(7)
Na1	OW7	2.400(7)	Na2	OW1	2.492(7)	Na3	O4	2.234(7)
Na1	F2	2.540(20)	Na4	OW10	2.337(7)	Na3	O5	2.237(7)
Na1	F46B	2.574(19)	Na4	OW6	2.366(7)	Na3	OW5	2.403(7)
Na2	Na3	3.420(4)	Na4	O8	2.367(6)	Na3	F32	2.54(30)
Na2	OW3	2.329(7)	Na4	OW9	2.412(7)	Na3	F16	2.574(19)
Na2	OW2	2.370(7)	Na4	OW7	2.422(7)	Na3	F32B	2.670(20)

References

1. Krause, L.; Herbst-Irmer, R.; Sheldrick, G. M.; Stalke, D., SADABS. *J. Appl. Crystallogr* **2015**, *48*, 3-10.
2. Sheldrick, G. M., ShelXT. *Acta Crystallogr.* **2008**, *A64*, 112-122.
3. Sheldrick, G. M., SHELX2018-1. *Acta Crystallogr.* **2015**, *C71*, 3-8.
4. Spek, A. L., *J. Appl. Cryst.* **2003**, *36*, 7-13.
5. Farrugia, L. J., ORTEP. *J. Appl. Cryst.* **2012**, *45*, 849-854.
6. Maza, W. A.; Etz, B. D.; Schutt, T. C.; Chaloux, B. L.; Breslin, V. M.; Pate, B. B.; Shukla, M. K.; Owrutsky, J. C.; Epshteyn, A., Impact of Submicellar Aggregation on Reduction Kinetics of Perfluorooctanoate by the Hydrated Electron. *Environ. Sci. Technol. Lett.* **2022**, *9*, 226-232.